J Mater Sci (2012) 47:4716–4725
DOI 10.1007/s10853-012-6340-3

Composition segregation in semi-solid metal cast AA7075 aluminium alloy

S. L. George · R. D. Knutsen

Received: 17 October 2011 / Accepted: 13 February 2012 / Published online: 25 February 2012

Abstract The composition distribution and microstructural evolution associated with the characteristic globular grain structure in semi-solid metal cast AA7075 aluminium alloy has been investigated. The primary globular grains possess uniform composition over nearly 90% of their diameter with fluctuations only occurring in the near surface of the individual grains. The inter-globular regions are solute rich and contain non-equilibrium eutectic. The segregation pattern in semi-solid cast structures occurs over a much greater length-scale than the dendritic pattern prevalent in conventional castings and it is proposed that the distinction arises from predominant planar growth of the α-primary globular grains during the SSM conditioning stage. Examination of the in-grain structure using electron backscattered diffraction revealed a quasi-periodic fluctuation in misorientation that may have arisen from local perturbations on the planar solid interface as solidification progressed. Homogenisation prior to artificial ageing is severely compromised by the undesirable segregation pattern.

Introduction

The semi-solid metal (SSM) casting process can produce net-shaped parts with very low porosity levels, thereby providing a production process that is potentially competitive to conventional component machining processes. The key to the success of this casting technique is the development of its semi-solid state, which, combined with the globular morphology of the primary grains in the structure, leads to improved mould filling during high pressure die casting. In the case of the rheocasting process, the globular grains form during the turbulent mixing stage that occurs prior to the transfer of the SSM to the mould cavity [1]. Success in the production of SSM cast aluminium components for demanding applications, such as those in the aerospace industry, lies not only in the formation of the uniform globular structure and reduced porosity, but also in the ability to obtain mechanical properties that meet high performance requirements. Consequently, it is desirable to combine the attractive SSM solidification structure with age-hardenable compositions such as those belonging to the AA7xxx wrought series. The thixoforming process and subsequent heat treatment has been used successfully elsewhere to achieve near comparable mechanical properties to a wrought equivalent [2]. Notwithstanding the similarities in manufacturing principles, thixoforming is a two-step process using pre-formed billets as feedstock with larger cost implications, while rheocasting has the potential to offer a single-step, more cost effective processing route. Therefore, investigations into achieving similar properties through rheocasting are important.

The optimisation of the strength of age-hardenable alloys requires uniform solute distribution, which may be difficult to achieve during SSM casting of complex Al–Zn alloys owing to the segregation pattern that is developed in the cast structure. Solidification of alloys is accompanied by varying degrees of microsegregation of solute as a result of solute partitioning between liquid and solid phases during solidification and the inevitable non-equilibrium nature of solidification [3]. Equilibrium solidification assumes complete mixing in both liquid and solid at every stage of freezing. In conventional or ingot casting, mixing in the liquid is generally the result of diffusional mixing and leads to

S. L. George (✉) · R. D. Knutsen
Department of Mechanical Engineering, Centre for Materials Engineering, University of Cape Town, Private Bag, Rondebosch 7701, South Africa
e-mail: sl.george@uct.ac.za

non-equilibrium dendritic solidification. The solute segregation thus occurs on a length scale equivalent to the dendrite arm spacing. For the production of wrought alloys, the elimination of the segregation pattern is assisted by thermomechanical processing. However, in SSM casting, the mixing in the liquid is achieved by the stirring during slurry production and therefore the solidification conditions during pre-conditioning are quite different compared to conventional casting. The mechanisms involved in the formation of the globular grains during solidification affect the composition, morphology, size and distribution of the primary globular α-grains and the mixture of phases that occur in the inter-globular regions after solidification is complete. Therefore, the evolution of the as-cast structure during post-solidification heat treatment is affected by the pattern of events that occur throughout the casting process. The purpose of this study is to examine the extent of solute segregation in SSM castings and to establish the influence of the inherent segregation on subsequent homogenisation processes. To this end, the segregation patterns and grain morphologies were evaluated using thermal analysis and analytical microscopy.

Experimental procedure

The aluminium–zinc alloy AA7075 (Al–5.56%Zn–2.45%Mg–1.55%Cu–0.24%Fe–0.24%Si–0.18%Cr–0.15%Mn), normally produced via conventional ingot or slab casting, was selected for this investigation because of its high achievable strengths through precipitation hardening. Plate samples (100 × 55 × 6 mm) were prepared using the council for scientific and industrial research rheo-casting system (CSIR-RCS) [4]. A batch of the wrought AA7075 feedstock alloy was melted in a 20 kg resistance furnace and degassed with argon. The liquid metal was poured into a cup at a temperature of approximately 40 °C above the liquidus and a SSM processing temperature of approximately 50% were used. The sequence for casting was as follows: liquid metal was poured from the tilting furnace into a stainless steel processing cup (∼400 g) which was then manually transferred to a CSIR-RCS induction facility where it is simultaneously air cooled and stirred, via an induction electromagnetic field coil, for ∼100–120 s. The semi-solid temperature of the material in the cup is measured by thermocouples. Processing stops when the desired semi-solid temperature of 625 °C was reached (the temperature corresponding to ∼50% solid fraction, determined by DSC results). The cup is ejected from the coil and transferred to the high pressure die caster where it is die cast using a 130-ton press [5]. The samples were sectioned from the centre of the cast plates. Each sample was mounted in resin and prepared for microscopic examination using conventional metallographic preparation techniques. The final mechanical polish was performed using OP-S colloidal silica to provide a suitable surface for microscopical analysis. To characterise the segregation and composition distribution in the as-cast structure, scanning electron microscopy (SEM) techniques including backscattered electron (BSE) imaging, energy dispersive X-ray spectroscopy (EDS) and electron backscatter diffraction (EBSD) pattern analysis were used. The instruments used were a ZEISS EVO 60 and a FEI Nova NanoSEM.

The re-melting behaviour of the SSM cast metal was characterised using differential scanning calorimetry (DSC). Specimens were inserted in alumina crucibles in a Netszch STA409 thermal analysis system and heated at a constant rate of 10 K/min. Further monitoring of microstructure evolution as function of temperature was carried out by conducting in situ heating experiments using a purpose-built hot stage in a CAMSCAN MX2500 scanning electron microscope (School of Materials, University of Manchester, UK). Images were acquired at different temperature intervals. The diffusion and melting of the eutectic in the interglobular regions were tracked, as well as the change in porosity associated with the incipient melting of the solute.

EBSD orientation analysis was performed in the SEM using HKL system. The step size between data points was 0.5 μm. The boundary misorientation conditions were defined as: high angle grain boundaries (HAGBs) when the misorientation across a boundary was >15° and low angle grain boundaries (LAGBs) for misorientations of between 2°and 15°.

Results

Morphological features: as-cast structure

Figure 1 illustrates a polarised light micrograph of the characteristic SSM cast microstructure. The structure is predominantly composed of a homogeneous distribution of primary α-grains possessing a globular morphology and an average grain diameter of between 80 and 100 μm. Although the level of contiguity between the individual globular grains is high, there is frequent occurrence of inter-globular regions that contain much finer phase dispersions, including α-grains that are much smaller than the primary α-grains. As is often the case with net-shape casting, there is the occurrence of macro-segregation owing to the liquid enrichment at the surface of the casting, highlighted by the grain size variation and distribution variation between the centre and surface of the casting. This is indicated in Fig. 2. This is inherent to the SSM processing route, but focus of the present route is to examine the segregation effect on a much more local scale. The EBSD orientation map in Fig. 3 highlights the

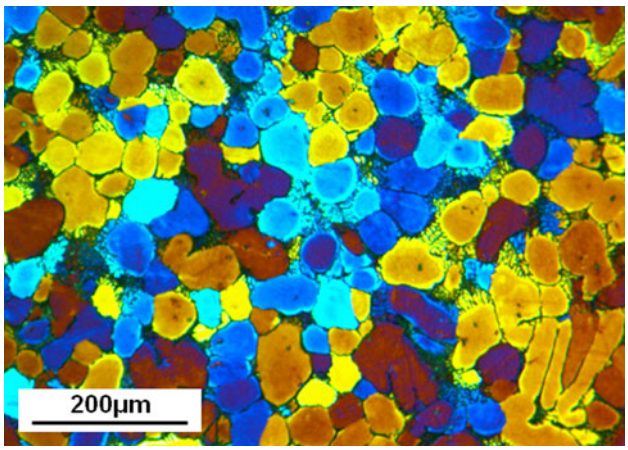

Fig. 1 Polarised light micrograph showing the globular α-grain structure of semi-solid cast AA7075

occurrence of the smaller α-grains between the primary α-grains. The colour map in Fig. 3 is a result of plotting individual Euler angles (φ_1, Φ, $\varphi_2 \leq 90°$) on an *XYZ* co-ordinate system defined by the conventional red, green and blue (RGB) scale and the sharp change in Euler colour generally indicates high angle grain boundaries. Low angle boundaries (LAGBs) can also be plotted by defining a minimum misorientation between neighbouring data points. In order to avoid noise associated with very low misorientations, only LAGBs misorientations, only LAGBs >2° are indicated as light grey lines in Fig. 3. The most notable feature is the in-grain boundaries that are visible in nearly all of the primary globular grains. These boundaries are mixed in character but the majority is represented by LAGBs, which tend to form "island-type" sub-grains within the primary globular grains. Teghtsoonian [6]

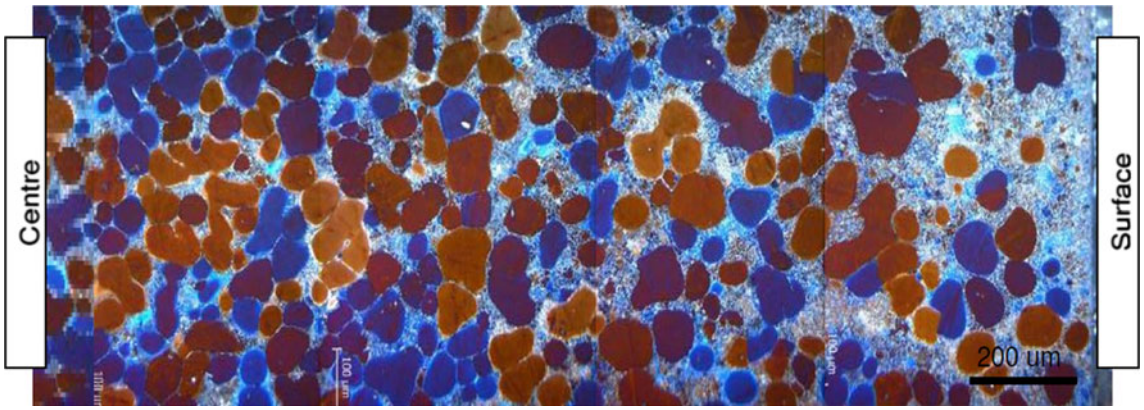

Fig. 2 Polarised light micrograph, showing the microstructural variation through the thickness of the SSM cast plate, from the centre of the thickness to the outer surface

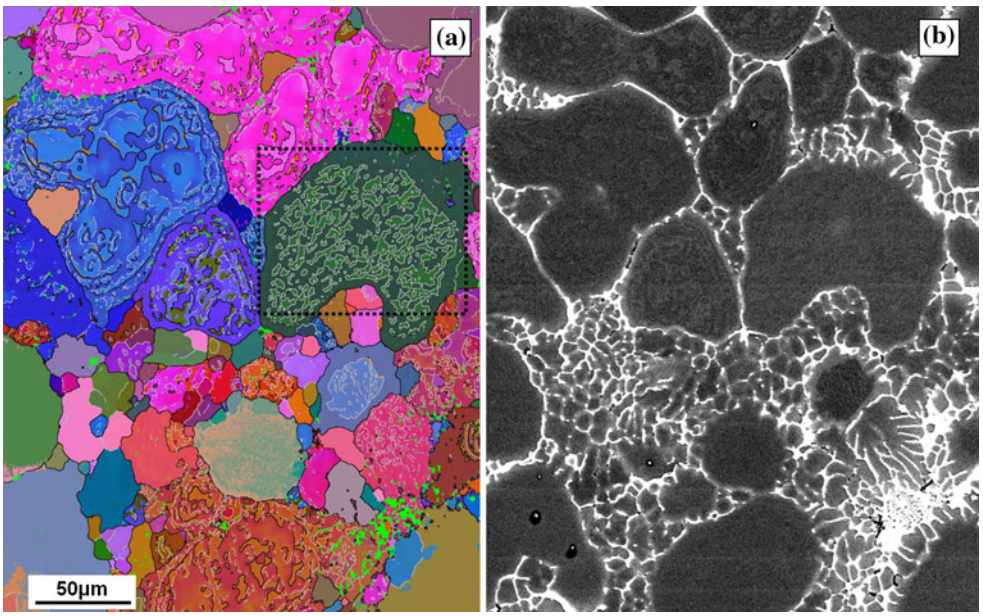

Fig. 3 **a** EBSD map shown in Euler colours with the HAGBs in *black*, the LA GBs in *grey* and **b** corresponding SEM BSE image

categorised this type of substructure as a "macromosaic structure", which was identified during the solidification of monocrystals that were composed of crystalline zones, slightly misoriented with respect to each other. The boundaries of these macromosaics formed as a result of the alignment of dislocations. Dislocations formed this way are arranged in a low-energy configuration thereby having greater stability at the high temperatures experienced during solidification as well as after prolonged annealing.

In addition to the smaller α-grains, a lamellar eutectic occurs throughout the inter-globular regions and is interspersed with minor microporosity. These features are exhibited in a higher magnification view (SEM image) of the inter-globular region in Fig. 4. The morphology of the porosity suggests that it was caused by shrinkage, which is also consistent with the association between the porosity and the eutectic structure. The eutectic forms at the end of the solidification sequence when the liquid supply is substantially constrained by the closed network created by the impinging globular grains [7]. Closer inspection of the polarised light micrograph in Fig. 1 indicates an outer contrast ring associated with the primary α-grain boundaries in many instances. The appearance of the contrast ring is explained by considering the composition distribution in the next section.

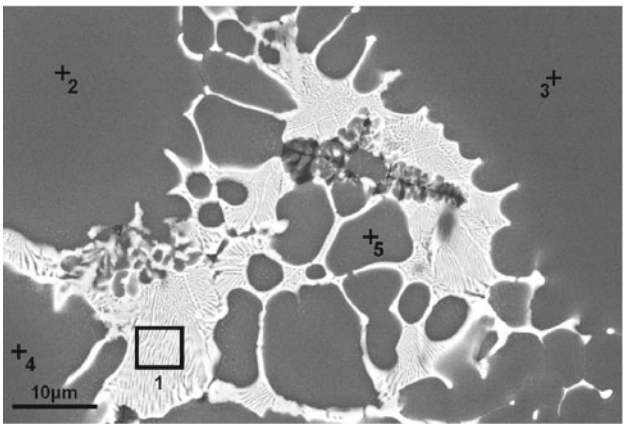

	Al	Zn	Mg	Cu
Point	Wt%	Wt%	Wt%	Wt%
1	41.5	30.2	14.8	13.1
2	93.9	4.3	1.3	0.5
3	94. 6	3.8	0.9	0.3
4	92.9	4.9	1.5	0.5
5	88.8	7.5	2.6	1.1

Fig. 4 SSM cast AA7075 alloy, showing the interglobular region between the α-grains. The table shows the composition of the five points marked on the image, as determined by EDS

Composition distribution: as-cast structure

It is quite understandable that there should be compositional variations associated with the different morphological features in the as-cast structure. The composition distribution along a line through a primary α-grain, whose boundary is intermittently delineated by eutectic, is shown by EDS elemental intensity graphs for aluminium, magnesium and zinc in Fig. 5. The general distribution indicates that the centre of the globular grain has a constant composition corresponding to location 1 (95 wt% Al, 1 wt% Mg and 3.5 wt% Zn). Towards the boundary of the globular grain the situation becomes different, indicated by the contrast ring noted in Fig. 1. The contrast change is due to the development of an outer coring ring manifest by a decrease in aluminium content and an increase in solute level. The composition within this coring ring is indicated by location 2 in Fig. 5 (93 wt% Al, 1.5 wt% Mg and 5 wt% Zn). As has been shown elsewhere [7], the final stages of the solidification of the primary α-grains can lead to the formation of cellular protrusions which extend from the edges of the grains when the growth is not impinged by neighbouring globules. The composition distribution continues to change from the coring ring into the protrusions, with the average composition shown by location 3 in Fig. 5 (90 wt% Al, 2 wt% Mg and 6 wt% Zn). The overall elemental distribution in Fig. 5 suggests that the major solute segregation occurs on a length-scale approximating the diameter of the primary α-grains. By contrast, the Zn concentration is measured across the dendritic structure in conventionally solidified AA7075 alloy, shown in Fig. 6. In the latter case, the initial melting and high pressure die casting conditions were identical to those employed for the SSM cast structure in Fig. 5 except that the SSM conditioning stage was omitted. Figure 6 shows the Zn profile across a number of dendrite arms and it is clear in this case

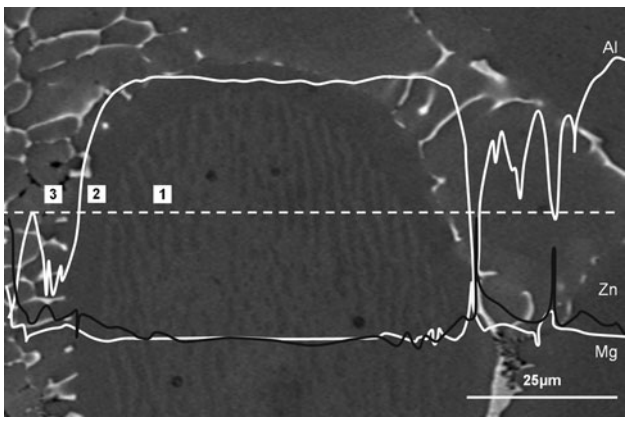

Fig. 5 EDS elemental intensity graphs for aluminium, magnesium and zinc of SSM cast AA7075, showing the composition distribution along a line through a primary α-grain

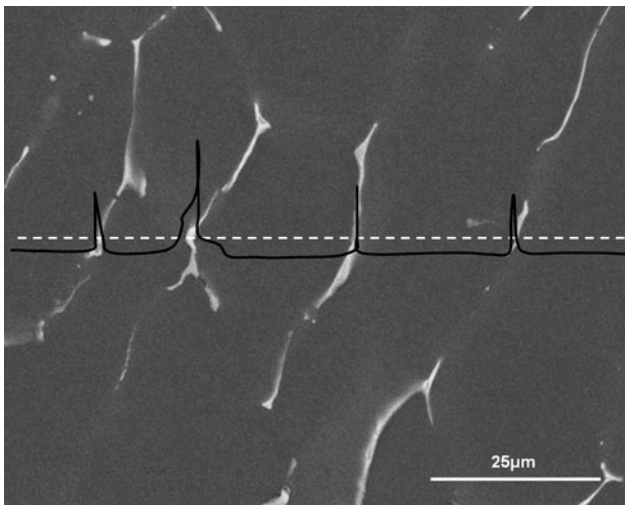

Fig. 6 Microstructure and zinc distribution in conventionally cast dendritic AA7075

that the level of Zn segregation is consistent with the average dendrite arm spacing. What is most significant, however, is that the average primary globular grain diameter is much greater than the dendrite arm spacing.

The composition of a number of points in Fig. 4 was measured by EDS in order to determine the extent of composition difference between the primary α-grains and the inter-globular region. Each beam spot analysis is marked with a "+" on the micrograph in Fig. 4 except for location 1 which indicates a small area scan encompassing a number of eutectic lamellae. The elements considered in the analyses for the AA7075 alloy were Al, Zn, Mg, Cu, Cr, Fe and Si and the corresponding wt% values are indicated in the table below the micrograph. The zinc-rich lamellar eutectic has a general composition ratio of 40:30 wt% Al to Zn, with Mg and Cu contents of approximately 14 and 13 wt% respectively. The eutectic of this alloy is reported to be composed of α-Al and $MgZn_2$ [8], although in some instances the Zn can be substituted by Cu atoms in the lattice, resulting in a higher Cu content value. This substitution can be made with extended composition ranges, namely $Mg(Al, Cu, Zn)_2$ [9]. The globular grains (points 2, 3 and 4 in Fig. 4) have typical compositions of approximately 94 wt% Al and 4 wt % Zn. The composition of a homogenised sample of AA7075, prior to semi-solid casting, has a Zn content of approximately 5.5 wt%. This degree of difference is a result of the solidification path of semi-solid casting and the resulting segregation. The smaller α-grain (point 5) within the inter-globular region has a much leaner Al content and richer solute content than the primary α-grains.

Microstructure evolution during reheating

The DSC trace that was acquired during reheating of the SSM cast AA7075 metal is presented in Fig. 7 and indicates that incipient melting of the zinc-rich phases initiates at 470 °C, which is below the normal homogenisation temperature range of between 480 and 500 °C for this alloy. In comparison, the same DSC experiment performed on wrought AA7075 demonstrates the first signs of melting at ~550 °C during reheating. The extent of solute segregation in the SSM cast metal is further highlighted by the fact that the major melting peak for the SSM cast metal starts at a higher temperature than the equivalent peak for the wrought metal. The DSC thermal analysis experiments for both the SSM and wrought samples were performed at a heating rate of 15 K/min.

A succession of micrographs which were acquired at 25, 360, 470 and 512 °C during reheating of the SSM cast metal in the SEM is presented in Fig. 8. The average heating rate between 400 and 512 °C during the in situ analysis was 1.5 °C/min. The selected area of interest focuses on the morphological changes associated with the inter-globular regions where the Zn-rich phases are identified by their bright atomic number (Z) contrast. Conversely, the BSE image exhibits dark contrast corresponding to microporosity. The porosity comprises a porous network within the solute-rich eutectic phases. The extent of incipient melting can be monitored by tracking the evolution of the porosity within the structure [10], where the surface area and morphology of the porosity changes with increasing temperature. During re-heating, melting occurs within the porous network (between the low temperature eutectic phases) resulting in a collapse of the porous network to produce a single large cavity. Thus the surface after incipient melting now reveals porosity which previously might have been immediately below the surface and hence concealed. In addition to emphasizing the presence of the Zn-rich eutectic phase, the Z-contrast of the BSE image also qualitatively indicates the Zn solute distribution within the α-grains. At 360 °C the contrast distribution has changed due to the local Zn enrichment of the α-phase consistent with the dissolution

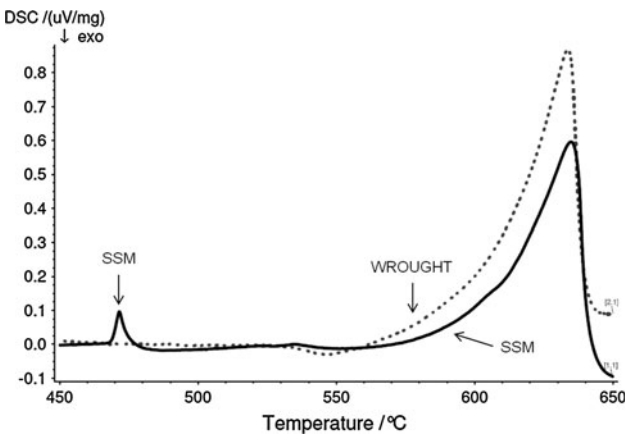

Fig. 7 DSC trace of a wrought AA7075 and SSM cast AA7075 alloy

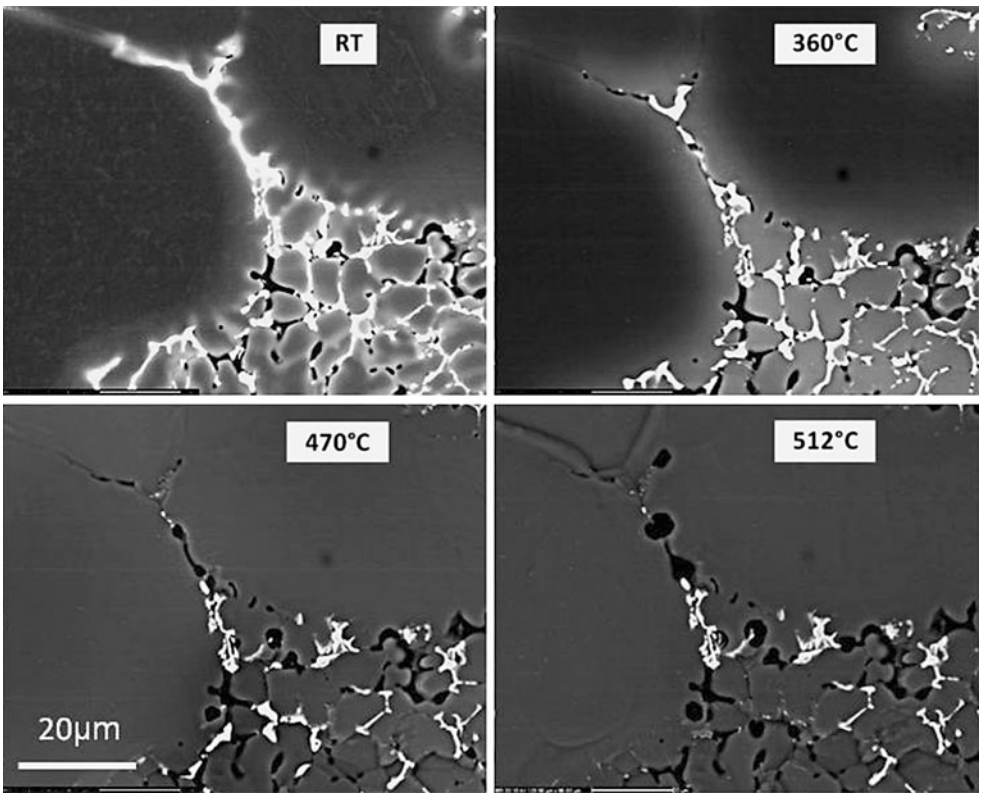

Fig. 8 Microstructural changes seen during in situ heating from room temperature through to 512 °C

of the Zn-rich eutectic phase. The morphology of the porosity has also altered as the surrounding eutectic is eliminated. Heating up to 470 °C eliminates the prior Z-contrast that is evident in the α-grains in the micrograph at 360 °C, thus indicating that extensive solute diffusion has occurred. The volume fraction of the Zn-rich eutectic phase has decreased substantially with concomitant increase in porosity. Even greater increase in porosity is evident at 512 °C and the morphology of the porosity has evolved such that large rounded pores are visible in many cases. The Zn-rich eutectic phase has diffused or melted, leaving only high-melting temperature intermetallic phases in the inter-globular region. In general, it was observed that the porosity gradually increases in size at temperatures below 400 °C which can be attributed to diffusion of the solute from the eutectic surrounding the shrinkage porosity. There is a sudden increase in porosity at 470 °C which coincides with the incipient melting temperature of the Zn-rich phase as detected from the DSC analysis.

In order to determine the effect of the segregation distribution on the age hardenability of SSM cast parts, T6 heat treatments (solution treat, quench, natural age, and artificial age) were performed on three samples for comparison of final hardness values. The conventional solution treatment temperature of 500 °C is higher than the onset of incipient melting of the high solute eutectic phase. This is illustrated in the DSC curve in Fig. 7 and the in situ heating images in Fig. 8. The sudden melting of the eutectic will disrupt the homogenisation process, and thus result in insufficient diffusion of solute towards the centre of the globular grains. Fan et al. [11] have shown that during homogenization of an Al–Zn–Mg–Cu alloy at a temperature below the incipient melting temperature, the primary eutectic structures gradually dissolved into the matrix, and the fraction of coarse particles decreased with the increasing of holding time. But lower temperature homogenisation processes have little effect on the Cu- and Fe-bearing particles. Chena et al. [12] showed an improvement in the dissolution of the soluble constituents in an AA7055 alloy, with the use of two-step heat treatments, where the first step was a homogenisation step at lower temperatures for extended lengths of time, up to 50 h. This then allowed for a second higher temperature solution treatment step, for the complete dissolution of the constituent particles. Therefore a second, lower solution temperature was also investigated, and the effects on ageing and hardness values were compared. One SSM cast sample underwent the standard 500 °C solution treatment, while the other was solution treated at 460 °C, which is below the incipient melting temperature. The resulting T6 hardness values are compared to the hardness results of a wrought AA7075 sample. The T6 treatment was: solution treatment at 500 °C for 6 h (or 460 °C for 6 h), quench, a natural ageing

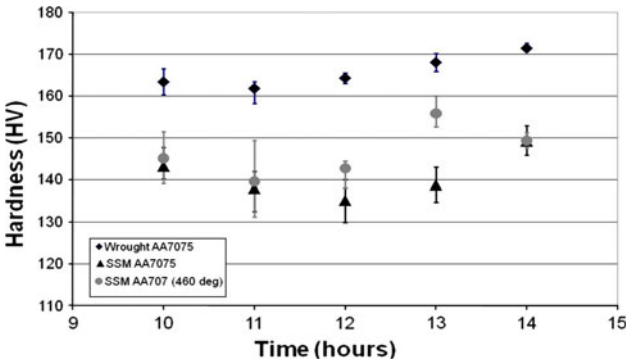

Fig. 9 Hardness curves for the T6 heat treatments for wrought AA7075, SSM AA7075 with a 500 °C solution treatment and SSM AA7075 with a 460 °C solution treatment

step at room temperature for 12 h and an artificial ageing step at 120 °C for 10–14 h. The graph in Fig. 9 demonstrates that the hardness values achieved for the SSM cast samples are well below those of the wrought samples. Although the SSM-460 °C sample achieved slightly higher hardness values than the SSM-500 °C sample, the SSM-cast hardness is consistently lower than the hardness developed in the equivalent wrought composition after the T6 heat treatment.

Discussion

The attractive primary α-grain morphology in the SSM as-cast state is without doubt undermined by the extensive elemental segregation associated with the inter-globular regions when casting complex alloys such as AA7075. On the one hand, the composition of the primary globular α-grains is uniform over more than 90% of the grain diameter with solute variations only occurring in the outermost rim and within the cellular protrusions which extend into the inter-globular region. The imposed turbulence during the SSM conditioning stage assists the mixing of the liquid and the more or less even composition across the primary globular grains suggests that a steady state condition exists at the solid/liquid interface. Nevertheless, the remaining liquid just prior to transfer to the die-casting station is enriched in solute and consequently leads to growth of the solute-rich rim around the primary α-grains which in some cases develop into cellular protrusions. Furthermore, solidification of solute-rich phases between the primary α-grains and the development of microporosity occurs. Of course this segregation pattern is not unusual in metal castings of any form, but the constant elemental composition over the primary α-grain diameter does lead to a much greater length-scale for subsequent homogenisation diffusion. This situation is easily understood when comparing the segregation profile for the SSM cast and conventionally cast conditions (Figs. 5, 6).

The microstructure behaviour during re-heating after solidification further emphasises the limitations imposed by the inherent segregation pattern. Despite the slow heating rate during the in situ SEM study, (1.5 °C/min between the temperature range of 400 and 512 °C) the retarded ability to homogenise resulted in localised melting of the eutectic phases in the same temperature range as that indicated by the DSC analysis (Fig. 7), where the heating rate was 15 K/min. Indicating within the range of 1–15 K/min, the heating rate has little effect on the location of the incipient melting of the solute-rich eutectic phases. The BSE contrast change in the image sequence during heating suggests homogenisation of the heavier elements (e.g. Zn) in the α-Al, but the growth in porosity as a result of localised melting develops a highly undesirable microstructure. Given this occurrence, it is imperative that homogenisation is performed below 470 °C. However, it is unlikely that this lower temperature will sufficiently heal the vast segregation inherent in the SSM cast AA7075 alloy. The dendritic form that is developed during conventional casting practice provides a shorter homogenisation length-scale and thus it may be stated that the level of segregation is much more acute in SSM castings and would require substantially longer homogenisation treatment in order to eventually meet the appropriate peak-aged condition, if this is indeed achievable. This is illustrated in Fig. 9, where the hardness values of the SSM samples after a T6 heat treatment are well below those of a wrought sample. The hardness values in Fig. 9 for the SSM sample where the solution treatment/homogenisation temperature was below the incipient melting temperature, were improved, but still below that of the wrought samples. This gives an indication that the segregation pattern was not fully homogenised prior to age hardening and this had a marked effect on the ageing process. The question now arises as to whether or not the very nature of formation of the desirable globular grain structure is a constraint in developing optimum properties in high performance age-hardenable aluminium alloys. To address this question, it is necessary to understand the mode of solidification of the globular grain morphology.

Several investigations have been reported which attempt to explain the solidification path that gives rise to the globular grain morphology, but there is often disagreement in the description of the events leading to globular solidification. Flemings et al. [13] proposed that the initial growth mode of the solid is dendritic and that shearing during the turbulent mixing stage causes fragmentation or bending of the dendrite arms thereby giving the resulting grains a rosette or globular morphology. Other proposals based on the dendrite arm fragmentation model attribute the fragmentation process to grain boundary induced melting as a result of solute-rich liquid attack at the root of

the dendrite arms [14, 15] and fragmentation of the arms owing to the shear stresses [16]. Later Mullis [17] proposed a model for the bending of the dendrite arms during growth in a sheared melt. In all these situations it is argued that dendritic solidification plays a major role. Much of the earlier work, however, is based on speculation and very little convincing experimental evidence is provided. More recent ideas tend towards the view that the globular morphology observed in semi-solid processing is as a result of planar or spherical growth under forced convection [18], or where the growth morphology changes from dendritic to spherical growth via rosette-type morphology during shearing [19] or, conversely, where the growth mode is never dendritic but is planar or cellular throughout [20].

The microstructural characteristics, including the morphology and distribution of the grains and specific features present in the as-cast structure, are evidence resulting from the solidification process itself and allude to the conditions at the solid–liquid interface and the solidification modes occurring during the casting process. In view of the differing opinions that have so far been expressed to account for the development of the globular primary grain structure, it is believed that more rigorous analysis of the structure of the primary grain will provide additional insight into the dominant solidification growth mode. The in-grain boundaries that are visible in nearly all of the primary globular grains (Fig. 3) are unusual and may provide some insight into the solid growth mode during the semi-solid condition stage of the SSM casting process. This subgrain morphology is highlighted further when plotted using relative Euler contrast in which the RGB levels are proportional to $(\varphi_1-\varphi_{1R})$, $(\Phi-\Phi_R)$ and $(\varphi_2-\varphi_{2R})$, where the subscript R denotes a reference pixel in the map [1]. A relative Euler contrast map of the region highlighted in Fig. 3 is presented in Fig. 10a. A profile of the cumulative misorientation along the line in the highlighted area illustrates the changes in crystal orientation associated with the transition across each of the in-grain boundaries (Fig. 10b). The pattern of these misorientations indicates quasi-periodicity which once again illustrates the "island" morphology of the subgrains. The LAGBs tend to disappear towards the edges of the globular grains, thus suggesting that they do not form during the final stages of solidification. The range of the relative Euler colours in the grain in Fig. 10a shows a fluctuation between two dominant orientations. The same orientation spread is also depicted in the {001} pole figure in Fig. 11, which is plotted for a data subset from Fig. 10a. The contour symmetry suggests a slight crystal rotation about a constant ⟨001⟩ direction, which is emphasised by the two superimposed triangles in Fig. 11.

The quasi-periodicity of the subgrain misorientations and the absence of the subgrain structure towards the rim of the globular grains implies that the subgrain structure forms during solidification at the turbulent mixing stage of the SSM casting operation. If this is true, then the misorientations must arise as a result of growth faults formed as the solidification front progresses. The connection between the formation of growth faults and solidification mode can be argued with reference to Fabietti and Travedi [21] who reported that faults, such as grain boundaries, form to relieve the lattice strain introduced during cellular growth. Cellular protrusions form as atoms add radially to furrows or nodes that develop on an unstable solid–liquid interface during solidification. It is proposed in our work that the formation of the boundary, as a result of the local radial growth of the protrusion, introduces a rotation of the growth direction of the solid, therefore resulting in a fractional deviation from the favoured ⟨100⟩ growth directions for aluminium [22], as depicted in the pole Figure in Fig. 11.

In describing the progression of solidification during semi-solid conditioning, it can be argued that the possibility of further growth or shrinkage of the cellular protrusions depends on the interaction between the solute and thermal fields in the melt and the interface of the solid protrusions. The conditions experienced during the turbulent mixing stage of the SSM casting process are such that the growth of the cellular protrusions is limited and, before a transition into dendritic growth is possible, the protrusions shrink, returning

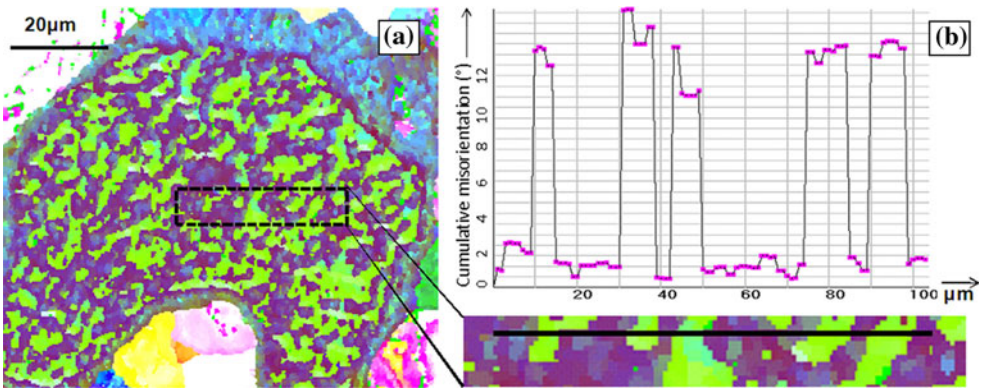

Fig. 10 **a** EBSD map of grain exhibiting the lamellar substructure configuration, shown in relative Euler colours, with **b** a misorientation profile corresponding to the *line* on the image

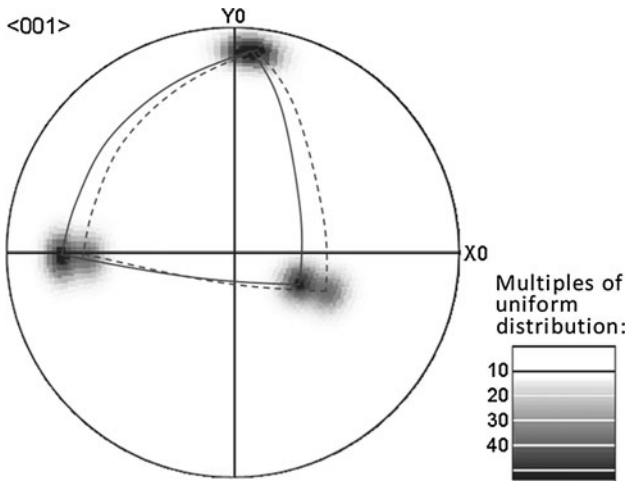

Fig. 11 Contour pole figure corresponding to Fig. 10

to a planar growth mode as the local solute and thermal conditions equilibrate temporarily during turbulent mixing. The variation in local conditions in the melt at the solid-front facilitates a constant change in solidification mode at the surface between planar and cellular. The schematic diagram in Fig. 12 shows the proposed fluctuation in solidification mode at the surface of the globular grain during solidification. At t_1 the growth mode is cellular. As solidification progresses through t_2 to t_3, the local conditions cause a shrinkage of the amplitude of the protrusions (the growth at the tips is retarded and the growth at the valleys is dominant) until a point where the front has become planar. At t_4 the growth mode returns to cellular as a result of instability at the interface owing to the fluctuation of conditions in the melt. It is suggested that the approximate wavelength of the protrusion, or cusp, profile at any instance during the solidification

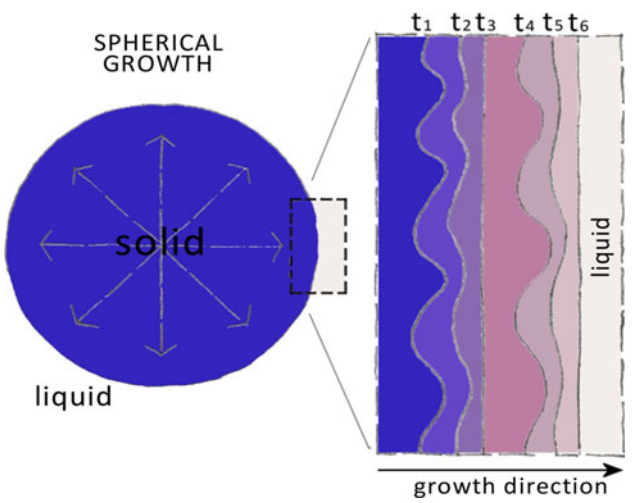

Fig. 12 Schematic illustration of the fluctuation of the growth mode at the surface of a globular grain during solidification

progression is defined by the quasi-periodicity of the orientation fluctuations demonstrated in Fig. 10b. There is thus a strong possibility that the evidence provided by the in-grain misorientations detected within the primary globular grains indicates that, even with the local fluctuations in growth mode between cellular and planar at the interface, the net overall growth mode of solidification during SSM processing is in fact planar, resulting in the characteristic globular grain morphology. Since it is highly unlikely that compositional equilibrium is obtained during solidification, the solute enriched liquid is concentrated between the large globular grains during the final stages of solidification, as opposed to the entrapment of liquid that one would expect between dendrite arms during dendritic solidification. Thus the SSM mode of solidification is akin to the condition where there is little or no diffusion in the solid and near-perfect mixing in the liquid. The result is the unavoidable segregation pattern exhibited in the SSM cast structure.

So far the in-grain boundary structure has only been analysed on a two dimensional surface. In other words, the EBSD orientation data presented in Figs. 3 and 10 provide a snapshot of a single instant in time as the solidification front progresses according to Fig. 12. Ideally, the ideas proposed in the article would be further substantiated if actual in-grain orientation data were obtained to directly support the full progression described in Fig. 12. Further study is presently under way that will attempt to characterise the three dimensional in-grain structure by combining serial sectioning and EBSD analysis in order to present a three dimensional view of the progression of the globular solidification front and hence expand on the schematic model presented in Fig. 12.

Conclusions

Detailed characterization of the morphology and composition of the SSM as-cast and re-heated microstructure has revealed the following:

- The solute segregation pattern that arises from the SSM die-casting of AA7075 generates solute segregation on a length-scale that is difficult to eliminate during post-solidification homogenisation.
- The concentration of low melting point eutectic between the primary globular α-grains further inhibits homogenisation by promoting porosity expansion at temperatures above 470 °C.
- Low angle grain boundaries within the globular primary α-grains provide evidence to support predominant planar growth of the advancing solid/liquid interface during the SSM conditioning stage.
- The planar growth mode accounts for the substantial solute enrichment in the inter-globular regions.

Acknowledgements The authors gratefully acknowledge the financial support of the National Research Foundation of South Africa (NRF), as well as the Council for Scientific and Industrial Research (CSIR) in Pretoria for the supply of samples.

References

1. Fan Z (2002) Int Mater Rev 47:1
2. Chayong S, Atkinson HV, Kaprinos P (2005) Mater Sci Eng A 390:3
3. Nadella R, Eskin DG, Du Q, Katgerman L (2008) Prog Mater Sci 53:421
4. Bruwer R, Wilkins JD, Ivanchev LH, Rossouw P, Damm OFRA, (2008) Patent number: US7368690
5. Curle UA (2010) Trans Nonferrous Met Soc China 20:1719
6. Teghtsoonian E (1951) Can J Phys 29:370
7. George SL, Knutsen RD (2011) JSAIMM 111:183
8. Fan X, Jiang D, Meng Q, Zhang B, Wang T (2006) Trans Nonferrous Met Soc 16:577
9. Deschamps A, Brechet Y, Livet F (1999) J Mater Sci Technol 15:993
10. Yang D, (2006) PhD Thesis, University of Quebec
11. Fan X, Jiang D, Meng Q, Zhong L (2006) Mater Lett 60:1475
12. Chena K, Liu H, Zhang Z, Li S, Todd RI (2003) J Mater Process Technol 142:190
13. Flemings MC, Riek RG, Young KP (1976) Mater Sci Eng 25:103
14. Vogel A, Doherty RD, Cantor B (1977) In: Proceedings of solidification and casting of metals conference, Sheffield, p. 518
15. Pilling J, Hellawell A (1996) Metall Trans A 27:229
16. Doherty RD, Lee HI, Feest EA (1984) Mater Sci Eng 65:181
17. Mullis AM (1999) Acta Mater 47:1783
18. Fan Z, Lui G (2005) Acta Mater 53:4345
19. Ji S, Fan Z (2002) Metall Trans A 33:3511
20. Molenaar JMM, Salemans FWHC, Katgerman L (1985) J Mater Sci 20:4335. doi:10.1007/BF00559322
21. Fabietti LM, Travedi R (1997) J Cryst Growth 173:503
22. Henry S, Minghetti T, Rappaz M (1998) Acta Mater 46:6431